J Electroceram (2009) 23:6–12
DOI 10.1007/s10832-008-9496-0

Effect of Cr additions on the electrical properties of Ni–$BaTiO_3$ ultra-thin multilayer capacitors

Anton V. Polotai · Tae-Hee Jeong · Gai-Ying Yang · Elizabeth C. Dickey · Clive A. Randall · Pascal Pinceloup · Abhijit S. Gurav

Received: 18 April 2007 / Accepted: 1 April 2008 / Published online: 6 May 2008

Abstract Multilayer ceramic capacitors based on $BaTiO_3$ dielectric compositions and Ni inner electrodes have complex interfacial reactions that impact the continuity of the inner electrode microstructure. Previously we demonstrated that through the addition of Cr to Ni, a significant improvement in the continuity of ultra-thin Ni electrodes in Ni–$BaTiO_3$ multilayer capacitors could be achieved. Here, the effect of the Cr addition to the nickel electrode pastes is studied with regard to the electrical properties. Low-field electrical measurements demonstrate no major differences between Cr doped Ni and undoped Ni. However, high-field measurements show a significant decrease to the total capacitor resistance. Under a critical electrical bias the conductivity significantly increases due to a Fowler–Nordheim tunneling conduction though the interfacial Schottky barrier at the dielectric–electrode interface; the onset voltage of this conduction is much lower than with the undoped nickel. Based on these results, we evaluate criteria for the selection of an appropriate refractory metal in order to improve the Ni electrode continuity.

Keywords MLCC · Nickel electrodes · $BaTiO_3$ · Ni–$BaTiO_3$ interfaces · Electrical properties

A. V. Polotai (✉) · T.-H. Jeong · G.-Y. Yang · E. C. Dickey · C. A. Randall
Department of Materials Science and Engineering,
Center for Dielectric Studies, The Pennsylvania State University,
University Park, PA 16802, USA
e-mail: avp10@psu.edu

P. Pinceloup · A. S. Gurav
KEMET Electronics Corporation,
P.O. Box 5928, Greenville, SC 29606, USA

1 Introduction

Microstructural control in high capacitance multilayer ceramic capacitors is one of the present day challenges for increasing capacitive volumetric efficiency. One of the current issues in state-of-the-art base–metal electrode multilayer ceramic capacitors (BME MLCCs) with dielectric and electrode layer thicknesses around or below 1 μm is the discontinuity of Ni electrodes, which can affect the electrical performance and reliability of final products [1, 2]. Recently, our investigations revealed the formation of an interfacial low-melting point (Ni,Ba,Ti) alloy with a melting point as low as 1000–1150 °C at Ni–$BaTiO_3$ interfaces [3–6]. The reduction process to produce the metallic Ti and Ba components results from the presence of residual carbon content from the organics used in the tape casting and screen printing process steps. Ni-enhanced catalytic reactions in the oxidation of this residual carbon locally reduce the $BaTiO_3$ adjacent to Ni electrodes, and it is estimated that the effective local oxygen activities are equivalent to pO_2's orders of magnitude lower than that of the ambient atmosphere present in the furnaces or reactors [4]. During co-sintering at temperatures higher than 1000 °C, the interfacial liquid layer may accelerate kinetic mass transfer along the interfaces and is believed to contribute to the discontinuity of Ni electrodes.

In the first paper of this series [7], we hypothesized that suppression of the interfacial liquid layer formation is possible via the modification of Ni electrodes with refractory metal(s). Our experiments revealed that when there is a segregation of Cr ions at Ni–$BaTiO_3$ interfaces, the formation of the liquid (Ni,Ba,Ti) interfacial layer is suppressed during co-sintering, which leads to a significant improvement to the continuity of Ni electrodes. But at the same time, it was suggested that the Cr addition to Ni

electrodes increases the amount of oxygen vacancies in $BaTiO_3$-based dielectric layers.

In regard to the electrical properties, the most important properties for a capacitor device are the permittivity and leakage characteristics, which collectively contribute to the capacitance and resistance of the device. Realized from earlier studies on $BaTiO_3$-based multilayer capacitors, the main contribution to the total resistance of MLCCs (over 70%) comes from interfacial contact resistance between the dielectric and electrode layers [2, 8–10]. The potential barrier at the interface results from a mismatch between the work function of a metal electrode (ϕ_m) and a semiconductor (ϕ_{sc}). This is a much more important issue in nickel inner electrode capacitors than in the air-fired capacitors with precious metal alloy electrode chemistries. In the Ni-based MLCC a simple blocking Schottky barrier is illustrated in Fig. 1, for the case of an n-type semiconductor and when $\phi_m > \phi_{sc}$. There may be interfacial states that also contribute to a more complex interface, but this is not illustrated here. Additionally, double Schottky barriers can also exist at the grain boundary interfaces thereby aiding the total resistance across the dielectric layer.

Most of our knowledge to the defect chemistry is based upon the air-fired pure or doped $BaTiO_3$ that can be either n-type or p-type semiconductor depending on defect compensation mechanisms controlled by the oxygen partial pressure and doping concentration [11–13]. The pure and acceptor-doped $BaTiO_3$ show n-type conduction in the low pO_2 region, generally below 10^{-5}–10^{-9} atm, and p-type conduction in the high pO_2 region for the temperature range from 750 to 1100 °C. Ni–$BaTiO_3$ MLCC chips are usually sintered at 1200–1300 °C ($pO_2 = 10^{-9} - 10^{-12}$ atm), which is the n-type region with high electronic conductivity. The high-temperature sintering is followed by reoxidation at 800–1000 °C ($pO_2 = 10^{-8} - 10^{-9}$ atm) to reduce the amount of free electron carriers in the dielectric. A Schottky barrier between Ni and $BaTiO_3$-based dielectric is found in BME capacitors and is the consequence of the $BaTiO_3$ being an n-type semiconductor. If the reoxidation conditions were equivalent to those in studies involving air-fired materials we would expect the reoxidation to produce either an ionically-compensated dielectric or a p-type dielectric. The p-type $BaTiO_3$–Ni interface will have a hole accumulation and would show an ohmic contact [14]. Previous studies of BME-MLCC chips before and after the reoxidation treatment confirmed the formation of blocking Schottky barrier in either case [3, 5]. This means that the $BaTiO_3$-based dielectric is still n-type semiconducting even after the reoxidation treatment and different from the air-fired cases.

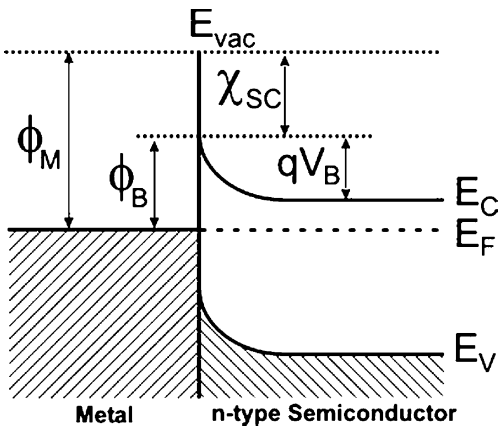

Fig. 1 Formation of Schottky barrier between a metal and n-type semiconductor, without pinning of the Fermi-level with interfacial states (Mott–Schottky contact) (after [8])

We also know that charged defects, like oxygen vacancies, can migrate toward the dielectric–electrode interface when DC-bias is applied and accumulate at the electrode regions [15–17]. In this case the formation of tunneling current through the Schottky barrier is possible, which will lead to significant suppression of interfacial contact resistance and degradation of total electrical properties [8, 10]. The formation of tunneling contacts will be discussed further throughout the text.

This paper discusses the effect of Cr addition on electrical properties of Ni–$BaTiO_3$ MLCCs and makes some suggestions about the possible changes in conductivity with and without the Cr addition. From these results we also suggest other alloy systems that could aid the design of the Ni-based MLCCs.

2 Experiments

The 0805-type MLCC green chips (1.60 mm×0.87 mm×0.90 mm, with 300 dielectric layers) were manufactured by KEMET Electronic Corporation, Greenville, SC, USA. Two types of MLCC samples, one with undoped Ni electrodes and another with 1 wt.% Cr-doped Ni electrodes were prepared by conventional tape casting techniques. The Ni–1 wt.%Cr alloy powder for this study was made by a flame-gas phase method. The thickness of electrode and dielectric layers were 0.9 and 1.2 μm, respectively. The dielectric was a $BaTiO_3$-based X5R-type material, which was formulated with chemical additives such as Y_2O_3 and MnO [18–21]. For binder burnout, the green chips were held at 220–280 °C for 20–30 h in a N_2–O_2 atmosphere. The green chips were subsequently co-fired in the temperature range from 1150 to 1250 °C for 5 h with 2.3 °C/min heating rate in a reducing atmosphere using an H_2O–N_2–H_2 gas mixture with pO_2 level from 10^{-9} to 10^{-11} atm at peak temperature. The pO_2 level was monitored by a zirconia-based oxygen probe made in-house and placed in a

vicinity of samples inside the furnace. The co-fired Ni–$BaTiO_3$ MLCCs were then cooled to a temperature range from 900 to 1100 °C at a 3 °C/min cooling rate and re-oxidized using an atmosphere with pO_2 level from 10^{-8} to 10^{-9} atm for 3 h.

To correlate electrical properties and compare insulation resistances of Ni–$BaTiO_3$ MLCCs with and without Cr addition, impedance spectroscopy (IS) and current–voltage (*I–V*) measurements were preformed. The real and imaginary components of the impedance were measured using a Solatron S11287 Electrochemical Interface and 1255B Frequency Response Analyzer (Solatron Analytical, UK). Impedance spectra with and without DC-bias were collected over a temperature range of 250 to 310 °C at 10 °C intervals. Each temperature of interest was held for at least 30 min to achieve thermal equilibrium before any measurements were taken. A 50 mV AC signal was applied over a frequency range 0.1 Hz to 1 MHz. The IS measurements with DC-bias (up to 10 V) were performed after allowing at least 3–5 min for current stabilization. Data were collected under a N_2 atmosphere to avoid in-situ oxidation of the end copper terminations of the MLCCs. The lowest measured temperature was limited by the impedance limit of the instrumentation (1 MΩ). Elevated temperatures were required to bring the sample resistance below this limit. Analysis and fitting of the experimental impedance data were accomplished using the electrochemical impedance software Z-plot and Z-view for Windows (Scribner Associates, Inc., USA). Experimental data were fitted with impedance models based on simple equivalent circuits.

The current–voltage (*I–V*) characteristics were measured at 130, 140 and 150 °C using a pA meter/DC voltage source HP-4141B (Hewlett-Packard, USA) in order to investigate leakage current behavior as function of applied field and temperature. Only the steady state leakage current was taken into account. In order to obtain steady state leakage current data, the current data were collected for at least 10 min at a constant DC-bias.

3 Results and discussion

Impedance spectroscopy is a very effective characterization tool to access the relative low-field lumped impedance contributions in a MLCC. Figure 2 presents complex impedance plots for undoped and Cr-doped MLCCs over the frequency range of 0.1 Hz to 1 MHz, at temperatures between 250 and 310 °C measured without a DC-bias. The shape of the impedance plot for the Cr-doped sample is found to be more distorted compared to the undoped one, with approximately 1.5 times higher total resistance. In the complex impedance plane, the intercepts of the impedance spectroscopy data with the real axis, *Z′*, correspond to the total resistance of the capacitor.

Generally, the total impedance of actual MLCCs is modeled by a series of leaky capacitive components for the dielectric–electrode interfaces (E), dielectric grains (G) and dielectric grain boundaries (GB) [5, 16, 22, 23]. The corresponding resistance for each element at low AC field (~50 mV), was calculated using this model and is summarized in Table 1. The IS data confirm the previously mentioned relationship $R_E > R_{GB} > R_G$, and indicate that dielectric–electrode interfaces play an important role in the control of the total insulation resistance of multilayer capacitors due to the formation of interfacial Schottky barriers. It should be noted that the fitting errors are estimated to be less than 5% for the undoped sample, whereas they increase to ~10% for the Cr-doped sample. This could be due to a heterogeneous distribution of Cr at the Ni–$BaTiO_3$ interfaces [7], which implies that the equivalent electrical network for Cr-doped sample may be more complicated.

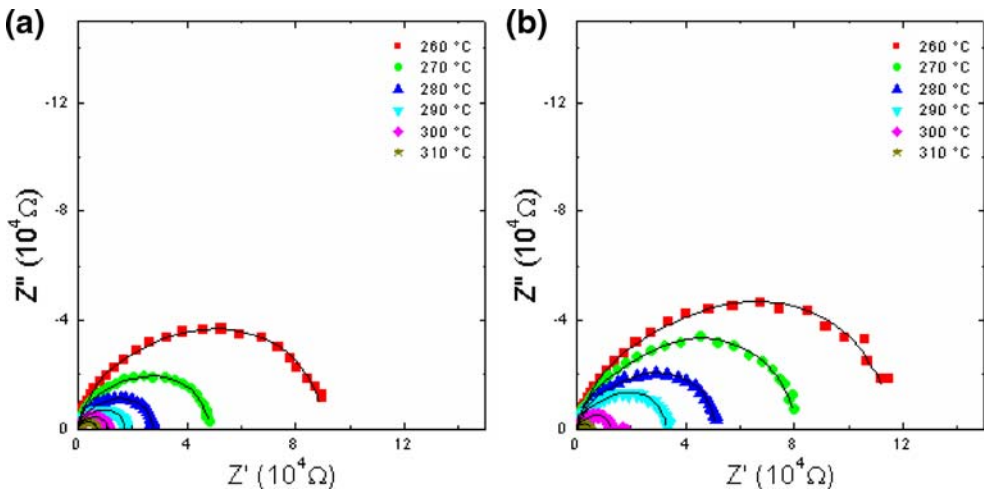

Fig. 2 Series of complex impedance plots for undoped (**a**) and Cr-doped (**b**) Ni–$BaTiO_3$ MLCCs, sintered at 1200 °C for 5 h

Table 1 Resistance of dielectric–electrode interfaces (R_E), dielectric grains (R_G) and dielectric grain boundaries (R_{GB}) for undoped and Cr-doped MLCCs sintered at 1200 °C for 5 h and measured at 260 °C without DC-bias.

	Total R, kΩ	R_E, kΩ	R_{GB}, kΩ	R_G, kΩ
Undoped MLCC	90.1±2.3	61.4±1.1	26.0±1.0	2.8±0.2
Cr-doped MLCC	113.3±3.6	84.7±1.7	25.8±1.6	2.7±0.3

The IS investigation with applied DC-bias revealed significant field dependence in the Cr-doped sample (Fig. 3), particularly for the electrode component and the grain boundaries at very low DC voltage ≤0.5 V. It is hypothesized that the DC-voltage induces local redistributions of oxygen vacancies, which migrates toward the cathode, and accumulate at Ni–$BaTiO_3$ interfaces [15–17]. In general, the depletion width, W, of the Schottky barrier is inversely proportional to the square root of the donor density near the interface [14, 15]. The local accumulation of oxygen vacancies n^+ facilitates a reduction of the Schottky barrier depletion width at the electrode dielectric interface, which alters the conduction mechanism from Schottky emission to tunneling, thereby enhancing the conduction [8, 10, 24]. Figure 4, shows a schematic diagram illustrating a Fowler–Nordheim tunneling contact. This is further supported with time dependant I–V measurements.

Figure 5 shows typical current variations with time for undoped and Cr-doped samples at 130 °C under an applied DC electrical field ~7.5×10^4 V/cm. Commonly, the time dependence of leakage current in dielectrics can be divided into three distinct zones: the initial depolarization zone, when the leakage current is decreased by the depolarization current, the steady state zone, and the final degradation zone, where the dielectric's resistivity degrades [16]. In the case of the Cr-doped sample, the degradation starts after a relatively short time ~1×10^3 s after the voltage was applied, whereas the undoped sample maintained its steady-state current orders of magnitude longer times.

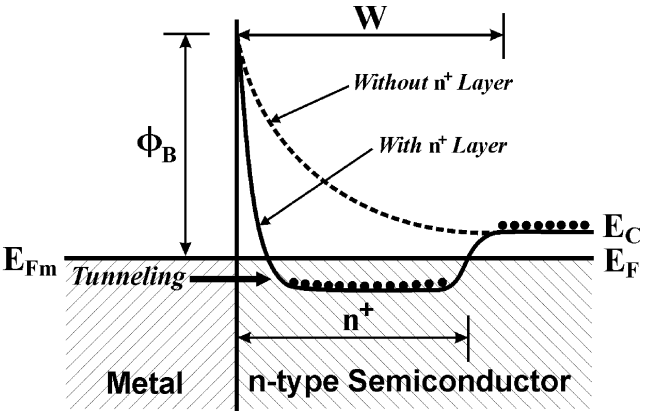

Fig. 4 Schematic presentation of Fowler–Nordheim tunneling of electrons through the Schottky barrier (after [14])

Figure 6 shows the steady state zone I–V data for undoped and Cr-doped MLCCs for temperature range between 130 and 150 °C; the data is plotted as (J/E^2 vs. $1/E$), a Fowler–Nordheim plot. For the undoped sample, the current density depends on temperature for the whole range of electrical fields investigated in this study. This is consistent with a thermionic emission current over the Schottky barrier [25, 26]. In the case of the Cr-doped sample, two regions can be distinguished. At low electric field, there is the temperature dependency of the current density, similar to that of undoped sample. At higher electric fields, the current density is almost temperature independent. When the applied DC field is larger than ~2.34 V/μm (DC-bias is ~2.8 V), the current density increases significantly, which is consistent with the IS measurements (Fig. 3). Also, the current density at high

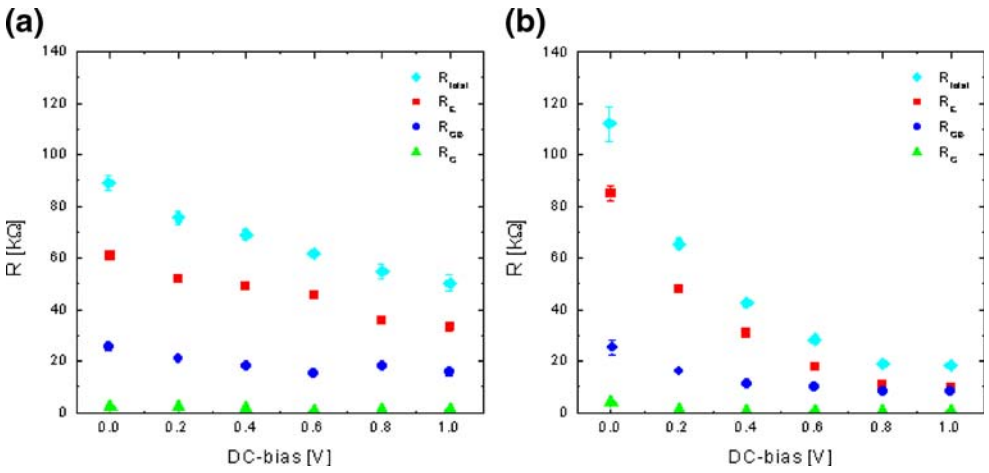

Fig. 3 Resistance variation as a function of applied voltage for undoped (**a**) and Cr-doped (**b**) MLCCs sintered at 1200 °C for 5 h and measured at 260 °C

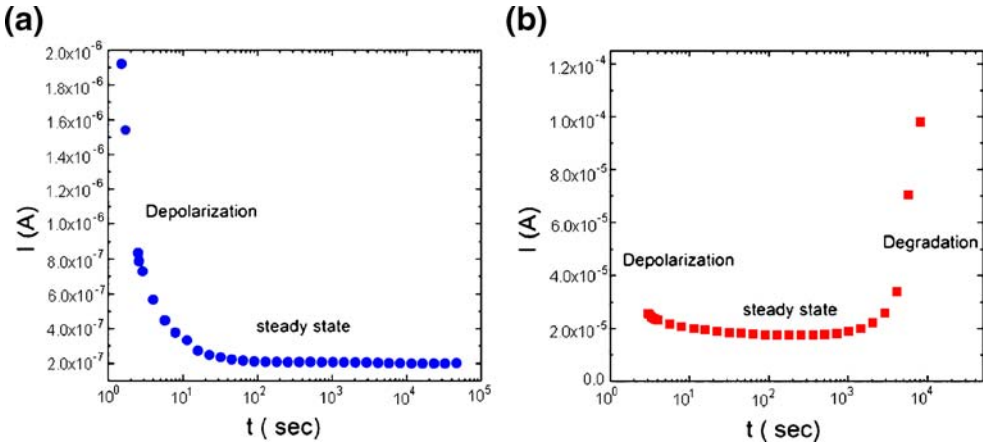

Fig. 5 Current variation with time at 130 °C under DC electric field ~7.5×10^4 V/cm for undoped (**a**) and Cr-doped (**b**) MLCCs sintered at 1200 °C for 5 h

electric fields was found to be almost temperature independent. Based on this data, it is reasonable to assume that the mechanism for electron injection from Ni into $BaTiO_3$ changed from thermionic emission to tunneling in the Cr-doped sample at high electric fields [14, 27].

In the thermionic emission region of the interfacial conductivity, the activation energy of the contact barrier (the effective Schottky barrier height) has been extracted for both types of samples using the $\log J/T^2$ vs. $1/T$ slope at fixed DC-bias (Fig. 7). A strong electrical field dependency on the activation energy is found for the Cr-doped sample, while the undoped sample shows only moderate field dependency (Fig. 8). In principle, the calculated activation energy of the contact barrier is expected to degrade abruptly when the tunneling current initiates. But in real systems, the transition from one conduction mechanism to another may become smoother due to the variation of metal–semiconductor interfacial microstructures, which was found by the high-resolution TEM investigation in Cr-doped MLCCs [7].

The conductivity through the Ni–$BaTiO_3$ interface is controlled by at least two factors: the Schottky barrier height and the concentration of mobile oxygen vacancies near the interface. The Schottky barrier height can be simply approximated as a difference between the work function of a metal (ϕ_m) and the electron affinity of a semiconductor (χ_{sc}). For Ni–$BaTiO_3$ multilayer capacitors it equals 1.25 eV (ϕ_{Ni}~5.15 eV [8, 28] and χ_{BaTiO3}~3.9 eV [15, 29, 30]). The formation of a metallic (Ni,Ba,Ti) alloy layer at the Ni–$BaTiO_3$ interface or segregation of Cr may reduce the Schottky barrier height because Ba, Ti and Cr have much lower work functions (ϕ_{Ba}~2.70 eV, ϕ_{Ti}~4.33 eV and ϕ_{Cr}~4.5 eV [28]) compared to Ni. The alloy (M_xm_{1-x}) work function can be approximated by the geometric mean of its components using Eq. 1, the so called Freeouf empirical model, that conveniently describes contact behavior at metal silicide interfaces [31]:

$$\phi^{\mathrm{Avg}} = \left(\phi_M^x \cdot \phi_m^{1-x}\right) \tag{1}$$

where ϕ_M and ϕ_m are the work functions of metal M and m respectively, and x is the concentration of metal M. Using the Freeouf relationship, the Schottky barrier height for the interfacial (Ni,Ba,Ti) and Ni–1 wt.% Cr alloys were estimated as 1.13 and 1.17 eV respectively compared to 1.25 eV for the pure Ni–$BaTiO_3$ contact. In spite of the simplicity of this model, it shows the same trend as the

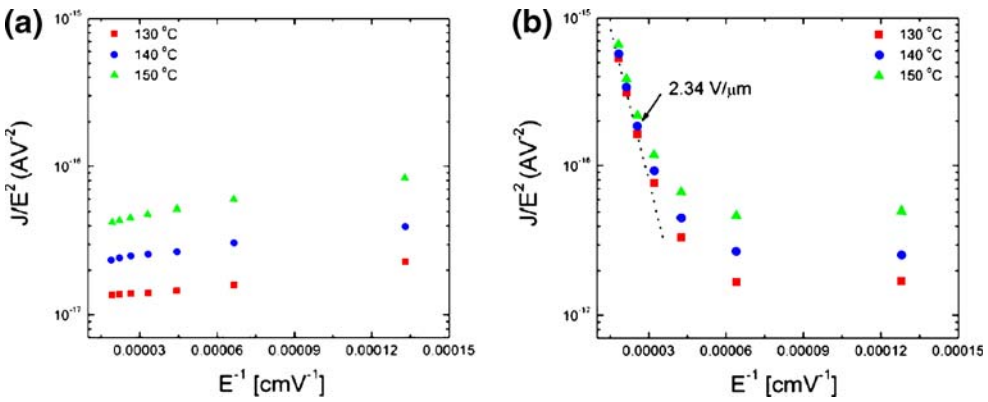

Fig. 6 Fowler–Nordheim plots for electrical conduction for undoped (**a**) and for Cr-doped (**b**) samples sintered at 1200 °C for 5 h. The *dashed line* in (**b**) shows the tunneling current according to the Fowler–Nordheim relationship, with the critical field being approximately 2.34 V/μm

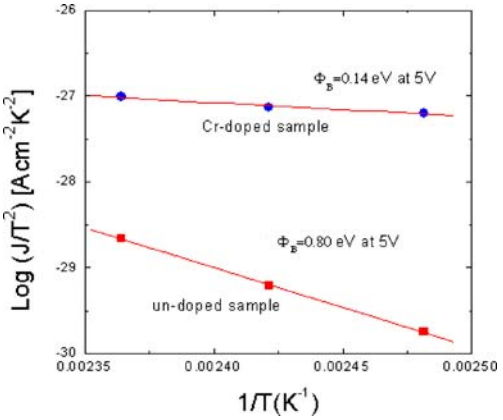

Fig. 7 Log (J/T^2) vs. $1/T$ plot for undoped and Cr-doped MLCCs at 5 V DC-bias

effective Schottky barrier height with Cr addition. The discrepancy between observed and calculated data most likely can be associated with the presence of defects like oxygen vacancies at Ni–$BaTiO_3$ interfaces.

In a previous paper [7] we showed that Cr was found not only at the Ni–$BaTiO_3$ interface. First, Cr was detected inside some of $BaTiO_3$ grains adjacent to the Ni–$BaTiO_3$ interfaces as a substituted acceptor ion. Cr to Ti substitution in $BaTiO_3$ is possible during sintering due to the similar ionic size between Cr^{3+} and Ti^{4+} ions $R(Cr^{3+})$= 0.755 nm, $R(Ti^{4+})$=0.745 nm [4, 32]. Second, Cr was also found as a separate Cr_2O_3 phase distributed at the Ni–$BaTiO_3$ interfaces. The formation of Cr_2O_3 most likely happened during the 3 h reoxidation treatment preventing full reoxidation of the $BaTiO_3$ due to the Cr having a much higher oxygen affinity compared to Ni and Ti: −1,135, −240 and −944 kJ/mol respectively [33]. Although the precise mechanisms are not fully understood, the net effect was a higher amount of oxygen vacancies in the $BaTiO_3$ compared to the undoped sample even after a general reoxidation treatment was performed. At high DC-bias, the oxygen vacancies migrate toward the cathode, suppress the space charge distribution of the Schottky barrier, and facilitate the electron tunneling through the barrier (Fig. 4), which drastically reduces the interfacial contact resistance (Fig. 8).

The selection of an appropriate doping element for improving the Ni layer stability and MLCC electrical properties is quite complicated. We have shown that the formation of the interfacial (Ni,Ba,Ti) alloy layer may reduce the effective Schottky barrier height at the Ni–$BaTiO_3$ interface. The segregation of Cr at Ni–$BaTiO_3$ interfaces suppresses the formation of the interfacial (Ni,Ba, Ti) alloy and significantly improves the continuity of Ni electrodes. But Cr also facilitates the formation of a high amount of mobile oxygen vacancies, which makes it undesirable for use in multilayer capacitors (Fig. 8). The appropriate refractory metal should have a high melting point, high affinity to Ni, Ba and Ti, a low affinity to oxygen, a significant work function equal to or higher than that of Ni and the restriction to act as an acceptor in the case of its diffusion inside the barium titanate lattice. The noble metals of the Pt sub-group may be considered as prospective candidates for the next generation of ultra-thin Ni–$BaTiO_3$ multilayer capacitors because they obey most of the abovementioned requirements. The future papers of this series will discuss the effect of noble metals additions as well as the effect of sintering kinetics on the continuity of Ni electrodes in Ni–$BaTiO_3$ MLCCs.

4 Conclusions

The investigation of the stability of Ni electrodes in ultra-thin Ni–$BaTiO_3$ multilayer ceramic capacitors reveals that the addition of Cr to Ni suppresses the formation of interfacial (Ni,Ba,Ti) alloy layer and improves the continuity of Ni electrodes. But, at the same time, it is found that Cr degrades the electrical properties of MLCCs. Low-field electrical measurements demonstrate no major differences between Cr doped and undoped Ni electrodes. However, high-field measurements show a significant decrease of the total resistivity. Under critical electrical bias the conductivity significantly increases due to a Fowler–Nordheim tunneling conduction through the interfacial Schottky barrier at the Ni–$BaTiO_3$ interface. Based on these results we evaluate criteria for the selection of appropriate refractory metal and propose that metals from the Pt sub-group may be considered as prospective candidates for the modification of Ni electrodes in novel Ni–$BaTiO_3$ MLCCs.

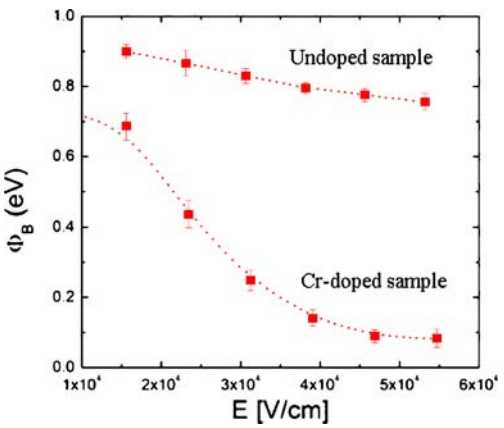

Fig. 8 Variation of the activation energy of the contact barrier with applied DC electrical field

Acknowledgments The authors acknowledge members of the NSF I/UCRC Center for Dielectric Studies and the Materials Characterization Laboratory at The Pennsylvania State University. This material is based upon work supported by the National Science Foundation, as part of the Center for Dielectric Studies under Grant No. 0628817.

References

1. C.A. Randall, J. Ceram. Soc. Jpn. **109**, S2 (2001)
2. H. Kishi, Y. Mizuno, H. Chazono, Jpn. J. Appl. Phys. Part 1—Regular Papers Short Notes & Review Papers **42**, 1 (2003)
3. G.Y. Yang, E.C. Dickey, C.A. Randall, D.E. Barber, P. Pinceloup, M.A. Henderson, R.A. Hill, J.J. Beeson, D.J. Skamser, J. Appl. Phys. **96**, 7492 (2004)
4. G.Y. Yang, S.I. Lee, Z.J. Liu, C.J. Anthony, E.C. Dickey, Z.K. Liu, C.A. Randall, Acta Mater. **54**, 3513 (2006)
5. G.Y. Yang, G.D. Lian, E.C. Dickey, C.A. Randall, D.E. Barber, P. Pinceloup, M.A. Henderson, R.A. Hill, J.J. Beeson, D.J. Skamser, J. Appl. Phys. **96**, 7500 (2004)
6. A.V. Polotai, G.Y. Yang, E.C. Dickey, C.A. Randall, J. Am. Ceram. Soc. **90**, 3811 (2007)
7. A.V. Polotai, T.H. Jeong, G.Y. Yang, E.C. Dickey, C.A. Randall, P. Pinceloup, A.S. Gurav, J. Electroceram. **18**, 261 (2007)
8. E.H. Rhoderick, R.H. Williams, *Metal–semiconductor Contacts* (Clarendon, Oxford, 1988)
9. Y. Sakabe, T. Reynolds, Am. Ceram. Soc. Bull. **81**, 24 (2002)
10. S.M. Sze, *Physics of Semiconductor Devices* (Wiley, New York, 1981)
11. N.H. Chan, R.K. Sharma, D.M. Smyth, J. Am. Ceram. Soc. **64**, 556 (1981)
12. D.M. Smyth, *The Defect Chemistry of Metal Oxides* (Oxford University Press, 2000), p. 304
13. C.R. Song, H.I. Yoo, J. Am. Ceram. Soc. **83**, 773 (2000)
14. H. Luth, *Surfaces and Interfaces of Solids* (Springer, New York, 1993)
15. D.P. Cann, C.A. Randall, J. Mater. Res. **12**, 1685 (1997)
16. H. Chazono, H. Kishi, Jpn. J. Appl. Phys. Part 1—Regular Papers Short Notes & Review Papers **40**, 5624 (2001)
17. M. Dawber, K.M. Rabe, J.F. Scott, Rev. Modern Phys. **77**, 1083 (2005)
18. K. Albertsen, D. Hennings, O. Steigelmann, J. Electroceram. **2**, 193 (1998)
19. C.C. Chou, C.S. Chen, I.N. Lin, W.C. Yang, H.F. Cheng, Ferroelectrics **332**, 35 (2006)
20. D. Hennings, G. Rosenstein, J. Am. Ceram. Soc. **67**, 249 (1984)
21. Y. Tsur, A. Hitomi, I. Scrymgeour, C.A. Randall, Jpn. J. Appl. Phys. Part 1—Regular Papers Short Notes & Review Papers **40**, 255 (2001)
22. D.E. Hennings, C. Hofer, R. Meyer, C. Pithan, Ceram. Trans. **167**, 319 (2005)
23. H.S. Maiti, R.N. Basu, Mater. Res. Bull. **21**, 1107 (1986)
24. S.B. Sinnott, E.C. Dickey, Mater. Sci. Eng. R—Reports **43**, 1 (2003)
25. S. Barth, U. Wolf, H. Bassler, P. Muller, H. Riel, H. Vestweber, P.F. Seidler, W. Riess, Physical Review B **60**, 8791 (1999)
26. C. Herring, M.H. Nichols, Rev. Modern Phys. **21**, 185 (1949)
27. N. Newman, M. Vanschilfgaarde, T. Kendelwicz, M.D. Williams, W.E. Spicer, Phys. Rev. B **33**, 1146 (1986)
28. D.E. Eastman, Phys. Rev. B **2**, 1 (1970)
29. N. Szydlo, R. Poirier, J. Appl. Phys. **51**, 3310 (1980)
30. D.P. Cann, J.P. Maria, C.A. Randall, J. Mater. Sci. **36**, 4969 (2001)
31. J.L. Freeouf, Solid State Commun. **33**, 1059 (1980)
32. H.W. Jaffe, *Crystal Chemistry and Refractivity* (Dover, Mineola, 1996)
33. C.H.P. Lupis, *Chemical Thermodynamics of Materials* (Elsevier, New York, 1983)